JACS
JOURNAL OF THE AMERICAN CHEMICAL SOCIETY

COMMUNICATION

pubs.acs.org/JACS

Preferential Binding of Peptides to Graphene Edges and Planes

Sang N. Kim,[†] Zhifeng Kuang,[†] Joseph M. Slocik,[†] Sharon E. Jones,[†] Yue Cui,[‡] Barry L. Farmer,[†] Michael C. McAlpine,[‡] and Rajesh R. Naik*[,†]

[†]Materials and Manufacturing Directorate, Air Force Research Laboratory, Wright-Patterson Air Force Base, Ohio 45433, United States

[‡]Department of Mechanical and Aerospace Engineering, Princeton University, Princeton, New Jersey 08544, United States

Supporting Information

ABSTRACT: Peptides identified from combinatorial peptide libraries have been shown to bind to a variety of abiotic surfaces. Biotic−abiotic interactions can be exploited to create hybrid materials with interesting electronic, optical, or catalytic properties. Here we show that peptides identified from a combinatorial phage display peptide library assemble preferentially to the edge or planar surface of graphene and can affect the electronic properties of graphene. Molecular dynamics simulations and experiments provide insight into the mechanism of peptide binding to the graphene edge.

In pristine graphene, the sp^2-hybridized C−C bonds of graphene's planar atoms possess a chemistry distinct from that of the relatively weak dangling =C−C(H)−C= bonds at the edges, enabling edge-directed covalent functionalization.[1,2] However, the irreversible nature of these covalent bonds can potentially hinder the electronic properties of graphene. Noncovalent methods employing $\pi-\pi$ interactions can be effective for plane-specific functionalization of graphene but are unsuitable for graphene edges.[3] Molecules that can be tailored to recognize either the planar surface or edges of graphene would be beneficial for modulating its properties. The physicochemical diversity of amino acids has led to the discovery of peptides that can selectively recognize a given material or surface as well as exhibit multifunctionality.[4−8] In this study, we demonstrate preferential edge- or planar noncovalent functionalization of graphene using peptides previously identified from a combinatorial phage display peptide library.[7,8] The peptides exhibit unique binding behavior toward graphene. Using molecular dynamics (MD) simulations, we demonstrate that the peptides bind to the planar surface or edge of graphene via $\pi-\pi$ stacking or electrostatic interactions, respectively. We also show that a bifunctional peptide designed from graphene- and gold-binding peptides can be used to direct the assembly of gold nanoparticles (AuNPs) to graphene edges. Electronic measurements using mechanically ablated graphene field-effect transistors (GFETs) suggest that the edge- and plane-binding peptides both affect the electronic properties of graphene. These and other similarly designed peptides may be useful in modulating the band-gap properties of graphene.

The graphene-binding peptide (GBP) with the amino acid sequence EPLQLKM was previously found to bind specifically to SLP30 graphite (Timcal, Westlake, OH; surface area = 8.0 m^2/g).[8] Since the majority of the SLP30 surface consists of graphene edges, an intriguing question we posed is whether GBP can selectively recognize graphene edges. To address this question, we exposed freshly cleaved highly ordered pyrolytic graphite (HOPG) samples to a solution containing GBP (0.5 mg/mL) for 15 min and then thoroughly rinsed them with deionized (DI) water. We analyzed the peptide-coated graphene sheets by atomic force microscopy (AFM), which showed that GBP preferentially localized and assembled close to the edges of the graphene sheets, forming aggregates with heights of ∼1 nm (Figure 1A). We carried out extensive AFM analysis to confirm that the peptide indeed assembled at the graphene edges preferentially (Figure S1 in the Supporting Information). In all cases, GBP was found to be present at the edges of the graphene sheets. The AFM phase images also showed clear contrast between the GBP assemblies on the graphene edges and the planar graphene surface (Figure S1).

In contrast, the dodecameric carbon nanotube-binding peptide (CBP) with sequence HSSYWYAFNNKT[7] was found to decorate the HOPG surface uniformly. As shown in Figure 1B, CBP forms a monolayer with distinct pores on the planar HOPG surface. The hollow pores had diameters of 20−90 nm (Figure S2). This was not unexpected, as the similarity in atomically exposed $\pi-\pi$ bonds in graphene and the carbon nanotubes should result in CBP binding. AFM analysis of the CBP-coated graphene sheets at the pores measured heights of 1−2 nm (Figure S2), which is similar to the height of the CBP monolayer coating observed on single-walled carbon nanotubes (thickness of ∼1.2 nm).[10] The pores created by CBP on graphene surfaces were formed as a result of drying effects (Figure S3). The topographical structures obtained were specific to the peptide coatings and not due to imaging of water-induced topological or phase changes[11] (Figure S4). To substantiate further the graphene-edge-binding capability of GBP, we made use of AuNPs as a label. AuNPs coated with GBP were able to localize at the edges of graphene. The bifunctional peptide GBP-A3 (EPLQLKM-GGGG-AYSSGAPPMPPF)[9] allowed us to synthesize 10 nm diameter AuNPs coated noncovalently with the GBP-A3 peptide. Bifunctional peptides have been used previously to demonstrate localization of nanoparticles onto specific surfaces.[7,8] The GBP domain should direct the AuNPs to the edges of graphene edges. The A3 peptide domain effectively binds to the AuNPs and can be fused to other peptide domains, such as the GBP domain in this case. Using freshly cleaved HOPG that was exposed to a solution of GBP-A3-coated AuNPs and then thoroughly rinsed with DI water to remove excess nanoparticles showed edge binding as well. As shown in Figure 1C, the majority of the AuNPs

Received: May 10, 2011
Published: August 24, 2011

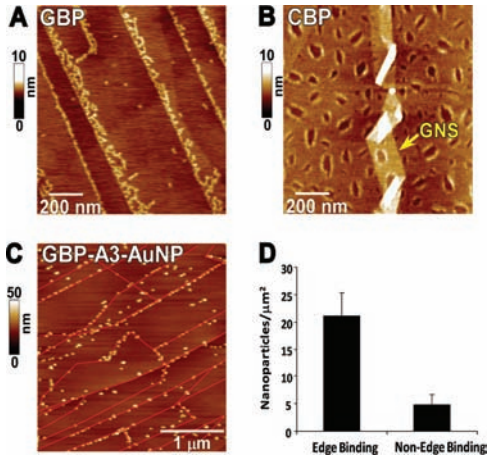

Figure 1. AFM topographic images obtained from graphene surfaces exposed to (A) GBP peptide and (B) CBP peptide, which assembled onto the graphene edges and plane, respectively. A graphene nanostrip (GNS) is indicated by the arrow. (C) AFM topographic image obtained from a graphene surface exposed to AuNPs functionalized with the GBP-A3 peptide (GBP-A3-AuNP), which assembled onto the graphene edge. Graphene edges (red lines) identified from sub-10 nm AFM height images are depicted for clarity. See Figure S2 for the corresponding phase images. (D) Bar chart showing the number of GBP-A3 peptide-functionalized nanoparticles binding to the edge and nonedge regions of graphene. The data were obtained by counting multiple regions in AFM scans.

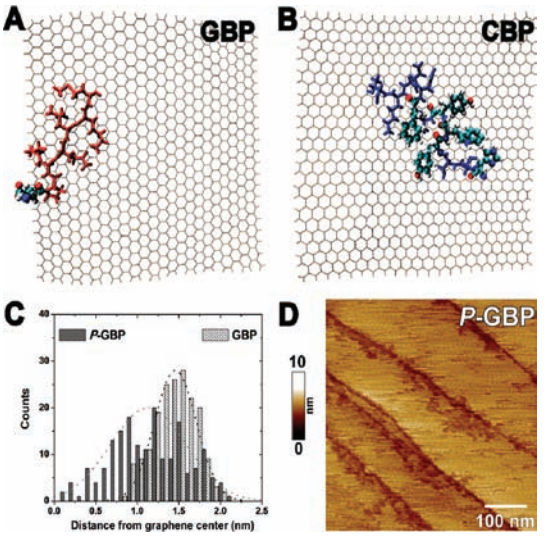

Figure 2. (A, B) Lowest-energy conformations of (A) GBP and (B) CBP obtained from six independent MD simulations started from plane center, near the zigzag edge, and near the armchair edge of a 5 nm × 5 nm model of graphene. (C) Mass center distribution histogram obtained from the MD simulations for GBP and protonated GBP (*P*-GBP), showing that GBP and *P*-GBP prefer to stay in proximity to the graphene edge and center, respectively. Normal distributions of the mass center are shown as dotted lines. (D) AFM topography obtained for *P*-GBP assembled on graphene/graphite at pH 3.

coated with GBP-A3 peptide were localized at the graphene edges, again emphasizing the edge-binding function of GBP, which was preserved even in the fusion peptide. We quantified the amount of edge versus plane binding of the GBP-A3-functionalized AuNPs by counting the number of AuNPs localized at edges and nonedges. The edges in the graphene surface were first defined by AFM height analysis and for clarity are indicated as red lines in Figure 1C. As shown in Figure 1D, ~80% of the peptide-coated AuNPs were found to be localized at the edges, while ~20% of the nanoparticles were randomly bound to the planar surface (nonedge) regions on graphene. AuNPs lacking the GBP domain but coated with the A3 peptide failed to bind to the graphene surface when similar deposition and rinsing methods were used (Figure S5). The edge-binding property of GBP can be further extended to other multifunctional peptide designs, which could be beneficial in the development of hybrid graphene systems for energy, catalysis, and sensing applications.

To elucidate further the binding properties of edge-selective GBP and plane-selective CBP, MD simulations of peptide–graphene complexes in explicit TIP3P water were performed. The GBP and CBP peptides were pre-equilibrated in TIP3P water and prearranged to six initial configurations in which the peptides were randomly positioned twice above the plane center, near the zigzag edge, or near the armchair edge of a ~25 nm^2 graphene model. Since the edge and other defect effects may be included in the charge density distribution of the graphene sheet, we explicitly assigned Mulliken partial charges to every atom using Gaussian 09.[12,13] Each system was energy-minimized for 2000 steps, heated to 300 K, and equilibrated for 20 ns using NAMD software.[14] The interaction energy was calculated every 100 ps along the trajectory after the simulations were terminated for each run. Figure 2A,B shows the most probable conformations of GBP and CBP on graphene after 20 ns equilibration (see Table S1 for the list of interaction energies). GBP was localized within 1.5 nm of the graphene edge with a weaker interaction energy (−109 kcal/mol), while CBP resided closer to the graphene center with a stronger interaction energy (−148 kcal/mol). The driving force for peptide binding to the edge or planar graphene surface could be attributed to electrostatic or $\pi-\pi$ interactions, respectively. Our computational studies indicate that GBP is attracted to the hydrogen-terminated positive graphene edge through the negatively charged glutamate (E) amino acid residue (shown using the ball-and-stick model in Figure 2A), whereas CBP extends its aromatic amino acid residues to maximize the ring–ring off-stack $\pi-\pi$ interactions[15] of the -H-Y-W-Y-F- residues (shown using the ball-and-stick model in Figure 2B) with the graphene surface, as previously shown by Kuang et al.[10] The MD simulations predicted that if the carboxylate group of glutamate (pK_a = 4.15) is in its protonated form, then GBP should be displaced from the edge-selective binding. When the equilibrated configurations were analyzed by calculating the distance from the center of mass of the peptides to the graphene center using 80 × 3 trajectory snapshots with 100 ps intervals (Figure 2C), the pronated peptide (*P*-GBP) was found to migrate away from the edge and move toward the center of the graphene sheet. We decided to test this experimentally by assembling GBP on graphene under acidic conditions (pH 3). The AFM images obtained from freshly cleaved graphene exposed to GBP under acidic conditions showed a different peptide binding behavior. GBP was found to be absent from the edges and deposited on the planar surface of graphene (Figure 2D and Figure S6). In contrast, binding of CBP to the graphene planar area was unaffected at low pH in both the computational simulations and AFM analysis (see Figure S7). This was not unexpected, as the association between CBP and graphene is due to $\pi-\pi$ interactions.[15] Computational results based on AutoDock 4.2[16]

dx.doi.org/10.1021/ja2042832 |*J. Am. Chem. Soc.* 2011, 133, 14480–14483

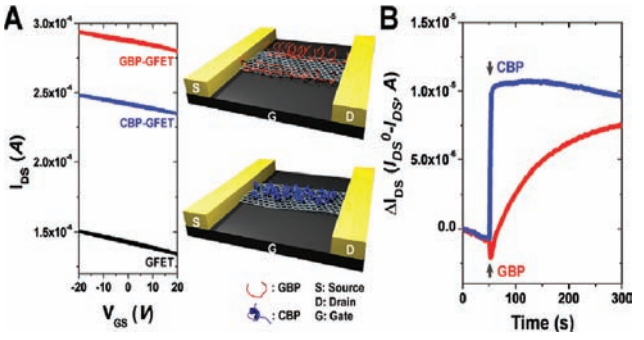

Figure 3. (A) Changes in GFET characteristics upon GBP or CBP binding. The scheme shows the corresponding CBP- and GBP-functionalized GFETs (290 nm thermal SiO_2 dielectric layer). (B) Real-time liquid-gated GFET I_{DS} measurements ($\Delta I_{DS} = I_{DS}^0 - I_{DS}$) in response to GBP or CBP (33.3 μM) binding. Arrows indicate the injection times for the GBP and CBP peptides.

also showed that the preferable distribution trends for the GBP and CBP peptides were also preserved on a larger 11.4 nm × 9.7 nm graphene model (Figure S8). Nonetheless, both modeling and the experimental results indicated that GBP and CBP have different binding behaviors and can be exploited to design other ligands that can preferentially bind to either the graphene edge or the planar graphene surface. More extensive mechanistic studies exploring the roles of various edge-chemical groups (carbonyl, hydroxyl, carboxyl, etc.), peptide variants, and multilayered graphene sheets are in progress to define further the binding behavior of the peptides.

The unique massless Dirac fermion characteristics in graphene exhibit similar wave function amplitudes for graphene edges and graphene planes.[17,18] Thus, the effect of edge functionalization of the pristine graphene is expected to play an important role in the modulation of its electronic properties. Edge functionalization can be used to modulate the band-gap properties of graphene by creating electron-scattering sites. We wanted to determine whether peptide binding to a graphene sheet in an FET device would change the electronic behavior of graphene. Graphene behaves as a p-type FET and upon binding to either GBP or CBP shows an increase in the electrical conductance indicating a p-type doping effect in the current gate field regime (−20 to 20 V).[19,20] Figure 3A shows the device output (gate voltage V_{GS} vs drain-source current I_{DS}) of the graphene FET before and after functionalization with GBP or CBP on the same graphene device (see Figure S9 for additional device measurements). Notably, the GBP peptide reproducibly increased the conductance of the GFET device relative to the CBP peptide. A higher degree of graphene p-doping by GBP than by CBP was observed by the G′ band shift in resonance Raman spectroscopy (RRS) mapping analysis of single-layer graphene samples (see Figure S10). While various factors, including the degree of oxidation of graphene by the peptide, can affect the electronic density of states in graphene, this result indicates that the binding of GBP to the edge affects the electronic structure of graphene more than when CBP binds to the planar graphene surface. Further studies using graphene nanostrip devices with defined aspect ratios should be able to provide better insights into the role of edge- and plane-binding peptides on the graphene density of states. Using the GFET device, we also measured the binding kinetics of GBP and CBP to graphene (Figure 3B) in the liquid-gate transistor configuration.[21,22] Exposure of GFET device to CBP resulted in a rapid change in conductance than that for GBP. Langmuir binding kinetics indicated the observed binding rate constant (k_{obs}) of CBP to be >40 times larger than that of GBP, which is consistent with the larger average interaction energy of CBP toward graphene in comparison with GBP, as observed with MD simulations. The binding behavior may also shed light on how the peptides assemble on the graphene surface. The rise in conductance in the presence of CBP may indicate a rapid accumulation on the graphene surface, whereas it appears to be much slower with GBP.

In summary, we have demonstrated the binding behavior of peptides onto mechanically exfoliated bulk graphene. GBP and CBP show differences in graphene binding, with GBP preferentially assembling at graphene edges. The formation of GBP aggregates at the edges is most likely due to high local peptide concentration. We have relied mostly on AFM, RRS, MD simulations, and electronic measurements to characterize the peptide binding on graphene because of the limitation of characterization tools with high resolution. In the future, scanning tunneling microscopy will be explored as a technique to study the ordering of the peptides on graphene surfaces. Nonetheless, our results open up a new facile method for functionalization of graphene nanosheets, micro/nanopatterns, and electronic devices. We hope that this study will result in further investigation of the use of peptides for asymmetrical functionalization of graphene and its use as a tool for modulating electronic properties. As graphene materials preparation and electronics fabrication technology advances, selective and controlled functionalization of graphene layers will benefit various electronics applications, such as in chemical sensors and biosensors.

■ ASSOCIATED CONTENT

Supporting Information. Experimental procedures, additional data, and complete ref 12 (as ref S3). This material is available free of charge via the Internet at http://pubs.acs.org.

■ AUTHOR INFORMATION

Corresponding Author
rajesh.naik@wapfb.af.mil

■ ACKNOWLEDGMENT

R.R.N. acknowledges funding support from the Air Force Office of Scientific Research. B.L.F. acknowledges the Materials and Manufacturing Directorate. M.C.M. acknowledges support of this work by the Air Force Office of Scientific Research via a Young Investigator Grant (FA9550-09-1-0096). We thank Laurie Wissler for providing technical assistance.

■ REFERENCES

(1) Sharma, R.; Baik, J. H.; Perera, C. J.; Strano, M. S. *Nano Lett.* **2010**, *10*, 398–405.
(2) Choi, E.-K.; Jeon, I.-Y.; Bae, S.-Y.; Lee, H.-J.; Shin, H. S.; Dai, L.; Baek, J.-B. *Chem. Commun.* **2010**, *46*, 6320–6322.
(3) Subrahmanyam, K. S.; Ghosh, A.; Gomathi, A.; Govindaraj, A.; Rao, C. N. R. *Nanosci. Nanotechnol. Lett.* **2009**, *1*, 28–31.
(4) Whaley, S. R.; English, D. S.; Hu, E. L.; Barbara, P. F.; Belcher, A. M. *Nature* **2000**, *405*, 665–668.
(5) Sarikaya, M.; Tamerler, C.; Jen, A. K. Y.; Schulten, K.; Baneyx, F. *Nat. Mater.* **2003**, *2*, 577–585.

(6) Fang, Y.; Wu, Q.; Dickerson, M. B.; Cai, Y.; Shian, S.; Berrigan, J. D.; Poulsen, N.; Kroger, N.; Sandhage, K. H. *Chem. Mater.* **2009**, *21*, 5704–5710.
(7) Pender, M. J.; Sowards, L. A.; Hartgerink, J. D.; Stone, M. O.; Naik, R. R. *Nano Lett.* **2006**, *6*, 40–44.
(8) Cui, Y.; Kim, S. N.; Jones, S. E.; Wissler, L. L.; Naik, R. R.; McAlpine, M. C. *Nano Lett.* **2010**, *10*, 4559–4565.
(9) Naik, R. R.; Stringer, S. J.; Agarwal, G.; Jones, S. E.; Stone, M. O. *Nat. Mater.* **2002**, *1*, 169–172.
(10) Kuang, Z.; Kim, S. N.; Crookes-Goodson, W. J.; Farmer, B. L.; Naik, R. R. *ACS Nano* **2010**, *4*, 452–458.
(11) Xu, K.; Cao, P.; Heath, J. R. *Science* **2010**, *329*, 1188–1191.
(12) Frisch, M. J.; et al. *Gaussian 09*, revision A.1; Gaussian, Inc.: Wallingford, CT, 2009.
(13) Case, D. A.; Cheatham, T. E., III; Darden, T.; Gohlke, H.; Luo, R.; Merz, K. M., Jr.; Onufriev, A.; Simmerling, C.; Wang, B.; Woods, R. J. *J. Comput. Chem.* **2005**, *26*, 1668–1688.
(14) Phillips, J. C.; Braun, R.; Wang, W.; Gumbart, J.; Tajkhorshid, E.; Villa, E.; Chipot, C.; Skeel, R. D.; Kalé, L.; Schulten, K. *J. Comput. Chem.* **2005**, *26*, 1781–1802.
(15) Tomaisio, S. M.; Walsh, T. R. *J. Phys. Chem. C* **2009**, *113*, 8778–8785.
(16) Morris, G. M.; Goodsell, D. S.; Halliday, R. S.; Huey, R.; Hart, W. E.; Belew, R. K.; Olson, A. J. *J. Comput. Chem.* **1998**, *19*, 1639–1662.
(17) Novoselov, K. S.; Geim, A. K.; Morozov, S. V.; Jiang, D.; Katsnelson, M. I.; Grigorieva, I. V.; Dubonos, S. V.; Firsov, A. A. *Nature* **2005**, *438*, 197–200.
(18) Nakada, K.; Fujita, M.; Dresselhaus, G.; Dresselhaus, M. S. *Phys. Rev. B* **1996**, *54*, 17954–17961.
(19) Bai, J.; Duan, X.; Huang, Y. *Nano Lett.* **2009**, *9*, 2083–2087.
(20) Liang, X.; Fu, Z.; Chou, S. Y. *Nano Lett.* **2007**, *7*, 3840–3844.
(21) Besteman, K.; Lee, J. O.; Wiertz, F. G. M.; Heering, H. A.; Dekker, C. *Nano Lett.* **2003**, *3*, 727–730.
(22) Kim, S.; Rusling, J.; Papadimitrakopoulos, F. *Adv. Mater.* **2007**, *19*, 3214–3228.